Int. J. Electrochem. Sci., 16 **(2021)** Article ID: 210322, doi: 10.20964/2021.03.66

International Journal of
ELECTROCHEMICAL
SCIENCE
www.electrochemsci.org

Transition metal oxide as possible electrode materials for Li-ion batteries: A DFT Analysis

S.Z.J Zaidi[1,3,*], *S.Hassan*[2], *M.Raza*[1], *F.C Walsh*[3]

[1] Institute of Chemical Engineering and Technology, University of the Punjab, Lahore, Pakistan
[2] Mechanical Engineering, Faculty of Engineering and Physical sciences, University of Southampton, U.K
[3] Electrochemical Engineering Lab, Energy Technologies, University of Southampton U.K
[*]E-mail: Zohaib.icet@pu.edu.pk

Received: 10 September 2020 / *Accepted:* 3 November 2020 / *Published:* 31 January 2021

To solve the problems of climate change and pave the way towards a more sustainable future, research is being done to find out new materials to be used in electrodes of high energy density batteries in different types of electronic equipment. Great efforts are underway to make new materials that can fulfill the requirements of the conditions for new batteries. The layered transition metals oxides are a new kind of material that are under consideration as new electrode materials for rechargeable Lithium-ion batteries. The layered transition metal oxides have garnered attention as a result of their lower production cost and relatively higher energy density that is associated with these materials..The old batteries get heated easily, which restricts their charging speed, and they are dangerous as they can explode due to their lower capacity range in the electronic vehicles arising safety concerns. There is a need to develop improved materials to provide affordable and heavy-duty batteries to employ in smart vehicles and gadgets.

Keywords: DFT, Graphene, Transition metal oxide, Li ion batteries

1. INTRODUCTION

We are facing unprecedented challenges of rising water levels and unbearable heat waves due to changing climate conditions.The electrification of everything is required from our cars to our devices of everyday uses. However, the batteries that are available now cannot meet the current challenges, and they heat up quickly, have low capacity andextremely low energy density as compared to fossil fuels, so new kinds of materials are being studied to meet these challenges [1-3,5-7]. We need to develop batteries with comparable energy density so that they can replace fossil fuels [8-13]. Some other transitional metals are also reported in the literature for different kind of batteries such as sodium ion and metal-air batteries where the electrode material is made up of transition metal oxides these batteries show excellent

results, performing much better than the traditionally produced lithium-ion batteries [4,14-16]. One of the significant advantages of transitional metals oxides is that they can be simply and cheaply synthesized on a large scale, so they can be readily produced to meet the demand on a large scale. Manganese oxide is the right candidate due to its large pseudo-capacitance but faces issues such as low electric conductivity and cation diffusivity [17]. That is why we introduced graphene which will compensate for these issues.

In this paper, A density functional theory (DFT) study was performed to further our understanding of the electronic structure of manganese dioxide as an electrode material for lithium-ion batteries and also better our understanding of how at the electron level MnO_2 and li-ions will interaction when graphene is introduced in the battery electrode material. Density function theory is used in computational chemistry modelling to check how molecules and compounds will act at the electronic level;the interaction of electrons helps in determining the properties of the said molecule [18-21]. We chose manganese dioxide as our candidate transition metal oxide due to its superior energy density, ease of synthesis, wide availability and safety, and it also forms a stable layered structure in the proposed molecular arrangement. Manganese dioxide has also been identified for use in super-capacitors [22-24]. We also used graphene in the design of the whole simulation;the graphene has a dual application. First, it provides a base for the manganese dioxide and second it also forms a bilayer with the other graphene to enclose the manganese dioxide. This forms a bi-layer which is known forimproving the properties of the battery [25-26]. Graphene is flexible, heat resistant, lightweight and has a high energy capacity. Graphene tends to improve the performance of battery electrodes [27-29]. Graphene has potential uses across many industrial sectors, from pharmaceuticals to semi-conductors to energy storage, and graphene usage has also shown to improve charge capacity and battery lifetime [30-32]. Nickel manganse cobal oxide (NMC) batteries which are the most used in electric vehicles nowadays are not safe due to the presence of cobalt and also is very expensive. The manganese oxide replaces cobalt in the current batteries [33-34].

In this paper, graphene has been introduced with MnO_2 to study how graphene's introduction improves the energy density and battery capacity[67] while also improving the stability of the electrodes for a long life cycle for a better battery performance[68-69]. The battery modeling was done to study the performance of the electrode material in a battery.

In table 2, we note various values of mass loadings and specific capacitance of different manganese and nanocarbon compounds such as graphene and carbon nanotubes (CNTs).In the electrochemical reaction, Li^+ ions are produced at the anode and interact with graphene and manganese oxide at the cathode during usage of the battery and reverse process happens during charging of the lithium-ion battery.

2. CALCULATION METHOD

The basis set selected for the optimization was B3LYP 6-31+G.The DFT functional will divide the electrical energy into various componets. The compound interaction with graphene was optimized to a minimum. Vibrational frequencies were calculated at the same level to locate the true minima. One

of the most accurate computing models was selected for this particular study.The Theoretical capacity of the battery is calculated from Faraday's laws:

$$Q_{theoretical} = (nF) / (3600*M) \quad mAh/g \qquad \text{(Eq. 1)}$$

The thoratical capacity of the material is calculated from equation 1. During the reaction at anode, the number of electrons produced will determine the capacity of the whole battery.The n, F and M are the number of charge carrier, the Faraday constant, 96, 485.3329 sA/mol and the molar mass of MnO_2 and graphene used in the electrode, respectively.

This density functional theory study was done through the simulation of manganese-rich compounds interaction with a nanomaterial which in this case,was graphene. The functions which are used in density functional theory are usually integrals of some function of the density and the density gradient[35-37]:

$$EKS = V + \langle hP \rangle + 1/2\langle PJ(P) \rangle + EX[P] + EC[P]$$

where EX[P] and EC[P] are the exchange functional and the correlation functional in the above equation, respectively.

Within the Kohn-Sham formulation, it can be regarded as a special case of density functional theory, with EX[P] given by the exchange integral -1/2<PK(P)> and EC=0. The functionals normally used in density functional theory are integrals of some function of the density and possibly the density gradient:

$$EX[P] = \int f(\rho\alpha(r),\rho\beta(r),\nabla\rho\alpha(r),\nabla\rho\beta(r))dr \qquad \text{(Eq. 2)}$$

The gradient is calculated, and the calculated values are then plotted in Fig. 7(b).The E_{homo}, E_{lumo}, E_{HLG} were obtained from the *Eigenvalues* and then converted into eV, The E_{HLG} was calculated by subtracting E_{HOMO} and E_{LUMO} values that were obtained from the simulation.

$E_{HLG} = E_{HOMO-} E_{LUMO}$

The Lithium ions were produced at anode as follows:

$2Li \quad \leftrightarrow Li^+ + e^-$

At Cathode:

$Li^+ + e- \leftrightarrow Li$

The reaction at anode determine the theoratical capacity of the electode.

3. RESULTS AND DISCUSSION

The initial model of the graphene and MnO_2 interaction with Li^+ ion is shown in Fig 1. A program was run before the final simulation to select the optimal interaction of the compounds with each other. The graphene and MnO_2 was optimized before the configuration's simulation was carried out. It is our observation that graphene provides the MnO_2 with a base to interact with Li^+ ion at the anode. This interaction of graphene and manganese allows intercalating and de-intercalating of the ion resulting in a better and smooth running of the battery.

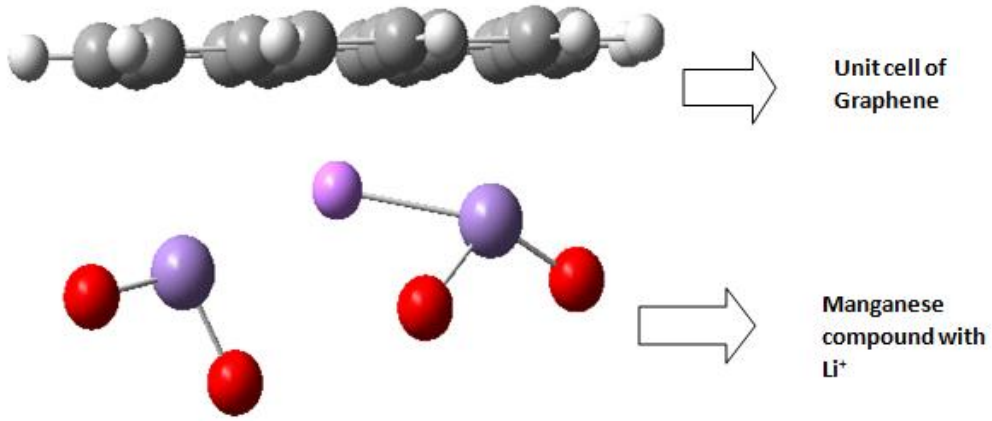

Figure 1. Interaction of MnO_2compound having Li^+ with a Unit cell of graphene.

3.1. Different Geometries of Optimized Structures

There occur a total of 7 intermediate geometries of the studied design. These intermediate as shown in Fig.2 geometries resonate from one position to another for a total of 7 different structures, and the result shows highly mobile lithium-ions, showing how easily the ions are intercalated and de-intercalated with the MnO_2. The combination of nano-structure of graphene and highly positive manganese results in a stable structure in which the li-ion can easily move between positive and negative electrode [50-51].

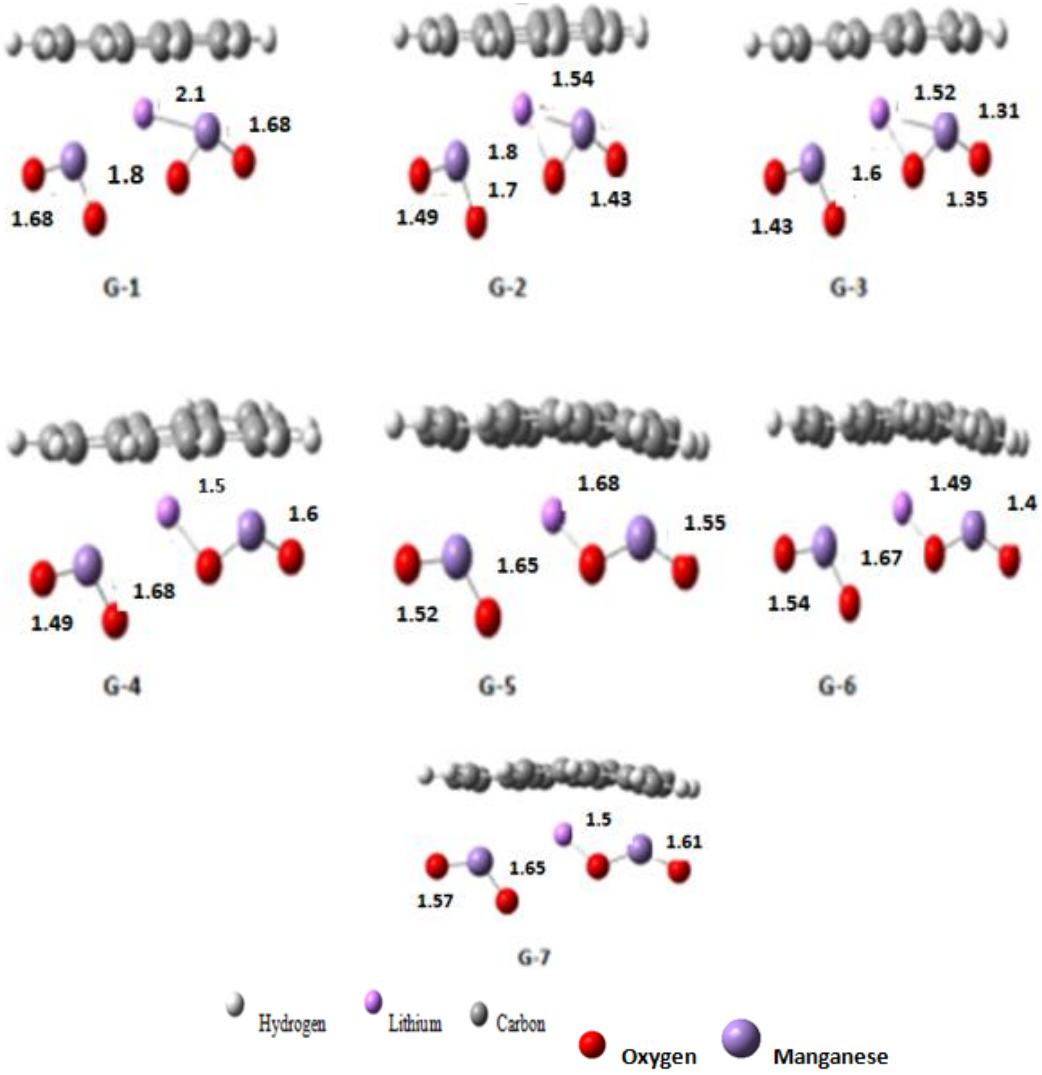

Figure 2. Intermediate geometries of the graphene, manganese and Li^+ ion. Bond length is given in Å. I.G were obtained at 25°C and 1 atm.

From Fig.2 it can also be seen that the bond length also changes somewhat dramatically, as a result of the resonant structure, which also results in a highly mobile Li^+ ion. This will result in a battery that can be very easily charged and discharged. From G-2 and G-3, we can observe that the interaction of Li^+-ion changes significantly with MnO_2, but the structure after it remains same, this represent an inherently stable structure of the whole MnO_2 with Li^+ ion in the presence of graphene. We can see from I.G 1 to I.G 7 the graphene is extremely stable, while the lithium-ion is interacting with MnO_2 compounds. These intermediate geometries show that while graphene is providing a stable base, the MnO_2 is interacting with the Li^+ ion.

3.2. Mulliken Charge

Mulliken charge occurs during Mulliken population analysis which is used in computational chemistry to show charge distribution in the compound that is being studied. The Mulliken population analysis was performed to show charge distribution which can be seen in Fig.3.

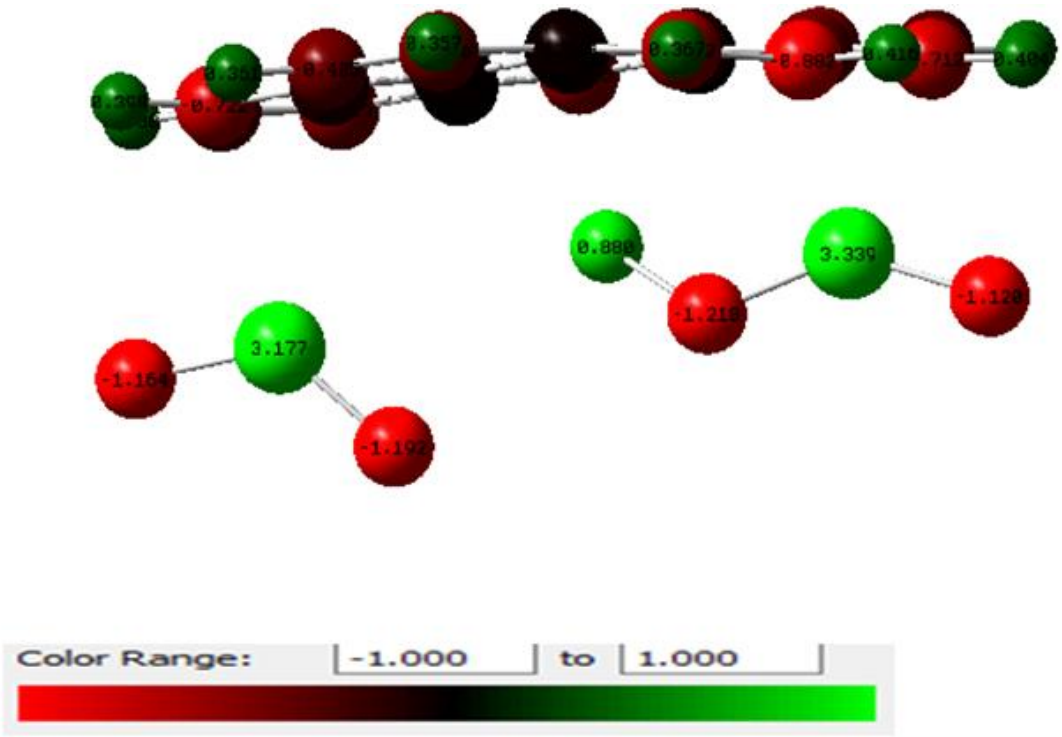

Figure 3. Charge distribution of the whole structure. The red means more electronegative and green means more electropositive Charge Distribution were obtained at 25°C and 1 atm.

Figure 3 shows the charge distribution. As manganese is also highly positively charged, the oxygen of the MnO_2 makes the Li^+ ion highly positive. So, the reason for the stable character that is observed in the structure is due to the presence of oxides. It can thus be reasonably inferred that other oxides of transition metals may also perform significantly well as electrode materials for electric batteries. MnO_2 in the configuration has highly negative oxygen which is why they are able to attract Li^+ which is highly positive ion. The center atoms in graphene in the configuration are extremely negative and as we move outward, the overall charge changes from positive to negative. A nano-sized manganese also possesses a high specific capacitance, which thus also improves the absorption of li-ion at the anode [52-54].

3.3. HOMO and LUMO

The HOMO and LUMO, as shown in Fig.4(a) and 4(b) illustrates the orbitals occupied by the electrons. The more red means the electrons concentration is higher at that place and green shows deficiency of electrons at that particular region.

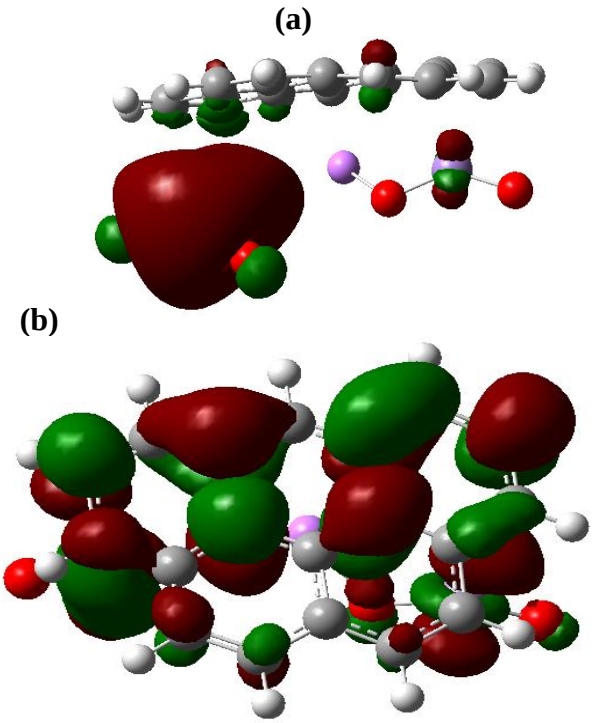

Figure 4. a) HOMO, **b)** LUMO electron distribution in whole structure. HOMO and LUMO were obtained at 25°C and 1 atm. Oxygen contain more electronegative charge.

From Fig.4 (a) it can be seen that the highly negative area are the oxygen compound surrounding the manganese atom, the lithium-ion is not affected by the whole electron distribution in the structure. In LUMO, the electrons are more evenly distributed throughout the whole structure. E_{HOMO} and E_{LUMO} were calculated to get the HOMO-LUMO energy gap. These values were calculated at STP. The E_{HOMO} was calculated to be -5.0344 eV, and the E_{LUMO} was -4.399 eV. The E_{HLG} was then obtained as 0.6354 eV. This is the excitation energy that is required for the electron to jump from LUMO to HOMO. As the energy is decreasing, so E_{HLG} shows us the stability of the arrangement. From the table 2 we can see that the Gibbs free energy and enthalpy of graphene-MnO_2 is more than either graphene or MnO_2. This increase shows a highly stable structure as more Gibbs free energy means, the process is less reversible. The HOMO and LUMO can also be used to find suitable functional electrolytes and how will oxidation affect them [40].

3.4. Internal Forces and Displacements

Figures 5 and 6 shown below give us the whole picture of the displacement and forces involved during the resonance of the intermediate geometries. They can tell us about the stability of the structure, mobility of the ions and the gradients which represents about the vectors of the intermolecular forces involved.

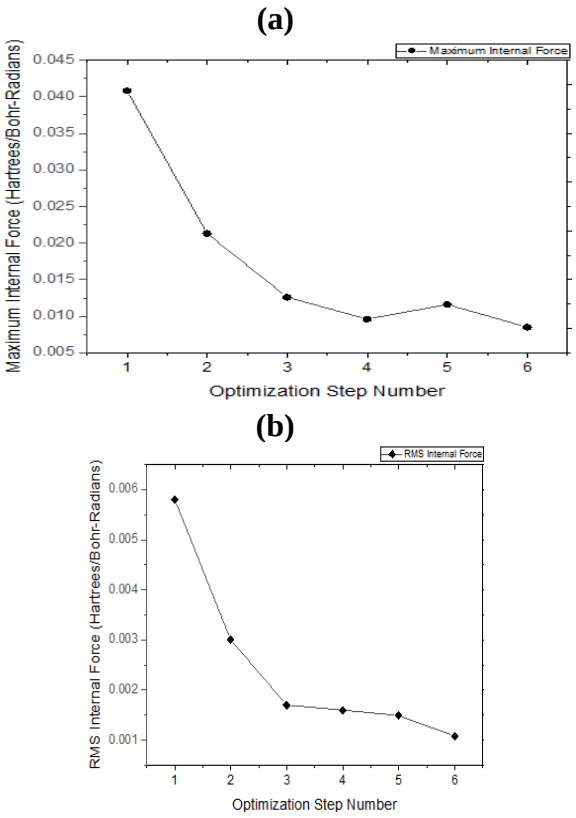

Figure 5. a) Maximum Internal force, **b)** Root mean square internal force related to the movement of Li ion inside the electronic structure

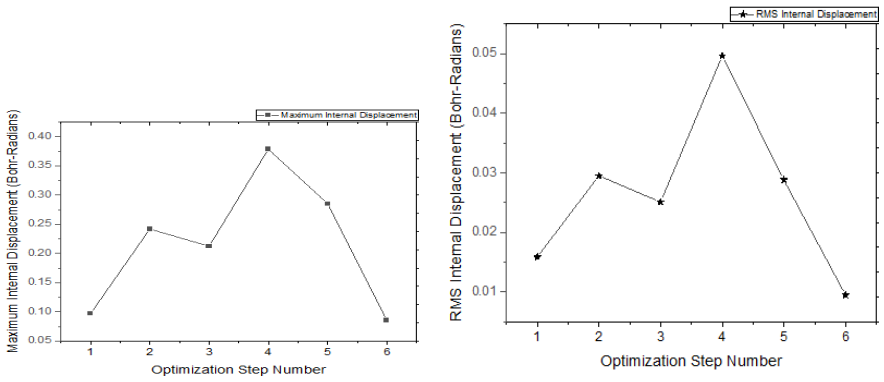

(a) (b)

Figure 6. a) Maximum Internal displacement, **b)**Root Mean Square internal displacement related to the movement of Li ion inside the electronic structure

The maximum an root mean square (RMS) internal forces are shown in Fig5(a)-(b). In Fig 5(a), the internal forces are constantly decreasing except at optimization step number 5, but in RMS, the forces are constantly decreasing until the final optimization step. It is due to the simulation condition that was

set to optimize the structure to a minimum. The internal forces are decreasing as the structure is optimized to obtain a highly stable structure of the whole arrangement finally.

The internal displacements, as shown in Fig.6 (a)-(b) of the internal resonance of the structure illustrate the free movements of the ion, particularly of the Li^+ ion. This mobility shows that the ions are easily intercalated and de-intercalated, which means that the batteries can be easily charged. The RMS internal forces show the gradient of the vectors of the compound. The internal forces increase or decrease at each optimization step which means that the whole structure is resonating at a single point. This single point provides for a highly stable structure while the continuous displacement of the whole structure provides for a highly mobile ion. The internal forces greatly affect the performance of li-ion batteries and these forces have a positive impact on the inner working of the batteries by the introduction of Manganese-oxide [55-56].

3.5. Total Energy and Gradient Norm

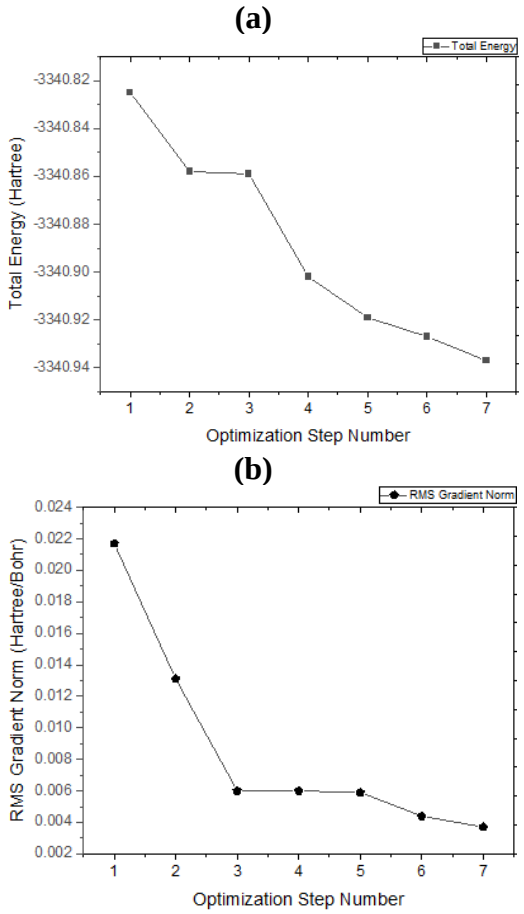

Figure 7. a) Total Energy, **b)** Root Mean Square Gradient Norm related to the movement of Li ion inside the electronic structure

Figure7 (a) shows the total energy continually decreasing as the optimization steps are increased except at 2 and 3, where the energy is almost the same. This same phenomenon can also be interpreted

from internal geometry at 2 and 3 where structures are different. The energy decrease after these steps is due to the fact that the structure is being optimized and energy is being lessened due to increased stability attained by the structure. In Fig. 7(b) the gradient norm tells us about the vector positions of the electrons in the structure. The decreasing gradient shows that the electrons are coming closer to each other. The vector position of the electrons is changing. The addition of graphene will further increase the capacity [64-65].

3.6. Battery Modeling

To understand how the electrode material would work in real life, a 3-D battery modeling was performed to accurately judge the results. Figure 8(a)- 8(b) shows the simple modelling structure. The li-ion battery model of Comsol Multiphysics is used. One of the most widely used LiPF6 as electrolyte with E.C(Ethylene carbonate).and D.M.C(Dimethyl carbonate) was used here in ratio 1:2. The E.C and D.M.C are the most used as binders in the li-ion batteries [60-62]. We will only deal with positive electrode where the interaction between manganese dioxide and lithium takes place with graphene at STP.

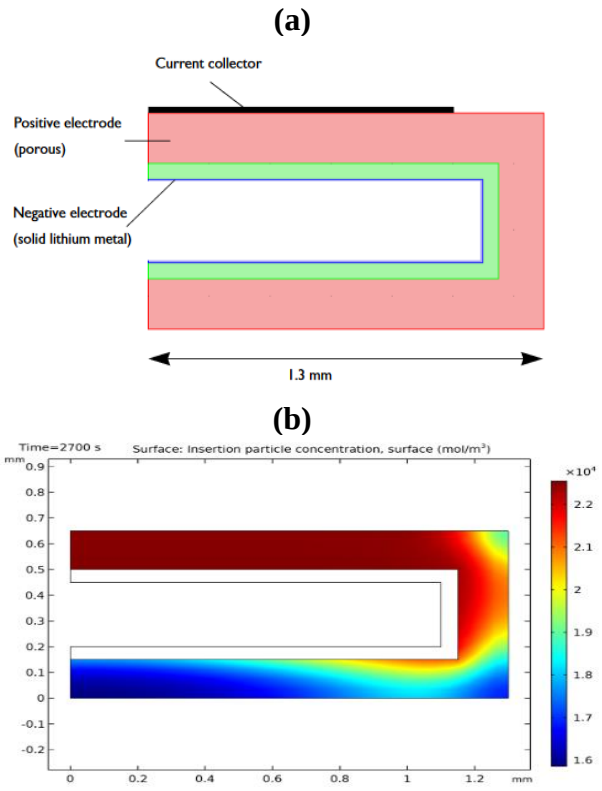

Figure 8. a) The 2-D structure with the negligible negative electrode, **b)** Lithium concentration at an electrode. Simulation was carried out at 25°C and 1 atm. High concentration of Li^+-ions at positive electrode is obtained during discharge cycle.

The extremely high lithium-on concentration shows when the battery is being discharged is shown in figure 8(b), while the negative electrode is kept to a minimum as we are focusing on anode for

evaluation of our configured electrode in the li-ion battery as shown in figure 8(a). The concentration of lithium was measured at 2700 seconds. The concentration, as can be seen, is extremely high at the positive electrode. This is during the discharge part of the running on the graph shown in Fig. 9, which shows the smooth discharge of the battery. The time-dependent model was used with standard battery running conditions. The battery discharges slowly at a stable voltage rate throughout all the discharge process.

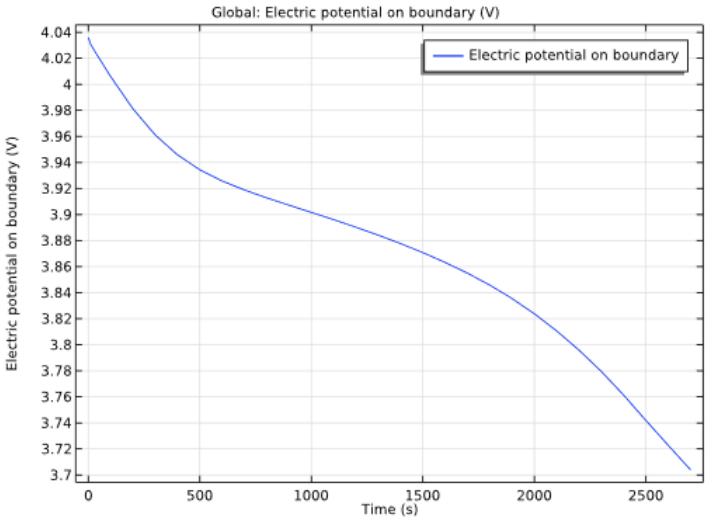

Figure 9. Discharge potenial of the Li ion Battery over time period of 2700 seconds. Simulation was carried out at 25°C and 1 atm. High concentration of Li^+-ions at positive electrode is obtained during discharge cycle.

3.7. Crystalline Structure

In previous DFT simulation we presented a single layer of MnO_2 interacting with lithium-ion at the positive electrode. In actuality, a crystal lattice is formed of MnO_2 which interacts with lithium-ion. The lattice is shown in Fig. 10 below. Crystal lattice has a great impact on migration of ions from positive to negative electrode and vice versa and the distorted layered structure provides an easy pathway for the movement of ions which results in a easy movement of ions [57-59].

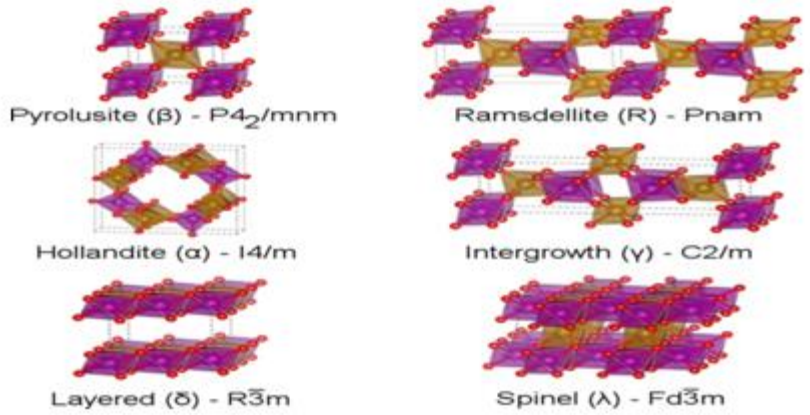

Figure 10. Crystal structure of MnO_2 polymorphs at the anode surface [38].

Due to the formation of the crystal lattice at the anode, the intercalation and de-intercalation of lithium-ions are feasible, and as a result, the battery can perform and last longer with a more extended range for electric vehicles. This structure of Manganese oxide is also very stable and safer than a conventional battery. The MnO_2 5th polymorph is intercalated in Fig.10 with lithium and graphene.

Table 1. The main calculated values of the MnO_2 battery. E_{HLG} value will tell us how much energy is required for an electron to move from a lower orbital to higher orbital and how much energy is released when an electron comes from a higher orbital towards a lower orbital.These values were obtained at 25°C and 1 atm.

E_{HOMO} eV	E_{LUMO} eV	E_{HLG} eV	$Q_{theoratical}$ W h/kg	V_{cell} V
-5.034	-4.399	0.6354	308	1.697

Table 2. Different types of MnO_2 Electrodes' experimental observed Specific Capacitance, Mass Loading and Energy density. The configuration discussed in this paper has the highest energy density of all the electrodes configurations noted in Table 2 The second highest value is noted for CNT/ MnO_2.

Electrode material	Mass loading Mg/cm^2	Specific capacitance F/g	Energy density Wh/kg	reference
Ultrafine manganese oxide decorated carbon fiber	0.1	179	19.7 at 0.25 A/g	41
MnO_2 reduced graphene coated carbon fiber	4	210 at 0.15 A/g	20	42
CNT loaded MnO_2	10	140	21	43

Activated Carbon only	10	180	3.6	43
Symmetric manganese oxide	10	160	1.9	43
Mn_3O_4 nanoparticles	0.37	98	17	44
LiMn2O4	2	137	56	45
Mesoporous MnO_2	2	87	32	46
MnO2- Carbon based polymer	3.7	45	43	47
Carbon cloth with T-Nb2O5@MnO_2	2.5	319.78	31.76	48
Multiwall CNTs/MnO_2	0.49	56	32.91	49
Pyrazine/graphene	/	/	107	This study

Table 3. Theoretical thermodynamics properties at standard temperature and pressure. Enthalpy, Gibbs Free energy and Thermal Energy of graphene stand alone, MnO_2 standalone and combined design values are noted below

Compound		Quantity	Value in kcal/mol
graphene	G		-2.09
	H		-2.64
	E		2.63
MnO2	G		-2.41
	H		-2.53
	E		2.55
graphene-MnO_2	G		-1.17
	H		-1.20
	E		3.01

6. CONCLUSIONS AND FUTURE CHALLENGES

In this paper we researched the benefits of layered transition metal oxides, we chose manganese dioxide as a transition layer oxide. One change in this paper was that graphene was introduced to make a bi-layer structure, like a sandwich with the transition metal oxide sandwiched between two graphene molecules. The results showed a highly mobile structure that allowed easy intercalation/de-intercalation of the li^+-ion in the whole battery; this will also allow for a fast-charging battery. The stability of the structure was also observed, meaning that the batteries produced with these materials will be safe.

Introduction of graphene also results in a lightweight battery which is another massive advantage of this material. This was a theoretical approach of designing new materials with the actions of the material observed in a fixed state and conditions, more practical studies should be done and compared with theoretical results to design better batteries.

ABBREVIATIONS:
Density Function Theory (DFT)
Becke-3 Parameter Lee
Yang and Parr (B3LYP),
Highest occupied molecular orbital (HOMO)
Lowest unoccupied molecular orbit (LUMO)
Highest occupied molecular orbital lowest unoccupied molecular orbit gap (HOMO-LUMO gap)
E_{HOMO} HOMO energy
E_{LUMO} LUMO Energy
E_{HLG} HOMO LUMO Gap Energy
RMS root mean square
$V_{battery}$ Voltage of battery
G gibbs free energy
H Enthalpy
E thermal energy
Q theoretical Theoretical capacity of the electrode

CONFLICTS OF INTEREST
The authors declare no conflict of interest.

References

1. Y. Hu, *Nature Energy*, 1 (2016) 16042.
2. J.W. Fergus, *Journal of Power Sources*, 195 (2010) 4554-4569.
3. K. Takada, *Acta Materialia*, 61 (2013) 759-770.
4. Q. Wang, S. Chu and S. Guo, *Chinese Chemical Letters*, 30 (2020) 2167-2176.
5. R. Yanbio, Z. Shichao, Z. Lincai and H. Xiowu, *Journal of Materials Research and Technology*, 9 (2019) 1549-1558.
6. H. Wan and X. Hu, *Solid State Ionics*, 341 (2019) 115030.
7. F. Wang, H. Yuan and J. Huang, *Journal of Alloys and Compounds*, 819 (2020) 153375.
8. W. Cao, J. Zhang and H. Li, *Energy Storage Materials*, 26 (2020) 46-55.
9. M.D. Leonard, E.E. Michaelides and D.N. Michaelides, *Renewable Energy*, 145 (2020) 951-962.
10. A. Fathy, H. Rezk and A.M. Naseef, *Renewable Energy*, 139 (2019) 147-160.
11. H. Raj, S. Singh and A. Sil, *Electrochimica Acta*, 326 (2019) 134981.
12. Y. Li, J. Yang and J. Song, *Renewable and Sustainable Energy Reviews*, 65 (2016) 685-697.
13. T. Kim, J. Lim, M. Oh and J. Kim, *Journal of Power Sources*, 361 (2017) 15-20.
14. R. Gao, Z. Zheng, P. Wang, C. Wang, H. Ye and F. Cao, *Energy Storage Materials*, 30 (2020) 9-26.
15. H. Lin, R. Jin, A. Wang, S. Zhu and H. Li, *Ceramics International*, 45 (2019) 17996-18002.
16. J. Do, I. Kim, H. Kim and Y. Jung, *Energy Storage Materials*, 25 (2020) 62-69.
17. T. Li, Y. Bai, Y. Wang, X. Hui and H. Jin, *Coordination Chemistry Reviews*, 410 (2020) 213221.
18. H. Farrokhpour and S. Khoshkhou, *Spectrochimica Acta Part A: Molecular and Biomolecular Spectroscopy*, 234 (2020) 118273.

19. S. Muzzafar, S. Imtiaz and S. Ali, *Journal of Molecular Structure*, 1217 (2020) 128419.
20. J. Conradie, *Data in Brief*, 30 (2020) 105617.
21. P. Santos and L. Veiros, *Tetrahedron*, 76 (2020) 131373.
22. A. Maheshwari, M. Heck and M. Santarelli, *Electrochimica Acta*, 273 (2018) 335-348.
23. V. Sridhar and H. Park, *Journal of Alloys and Compounds*, 808 (2020) 151748.
24. A. Eftekhari and F. Molaei, F, *Journal of Power Sources*, 274 (2020) 1306-1314.
25. S. Meng, *Energy Storage Materials*, 30 (2020) 296-328.
26. C. Senthil and C. Lee, *Data in Brief*, 30 (2020) 105472.
27. J. Knoop and S. Ahn, S, *Journal of Energy Chemistry*, 47 (2020) 86-106.
28. E. Demir, S. Soytas and R. Demir-Cakan, *Solid State Ionics*, 342 (2019) 115066.
29. M. Uddin, P. Alaboina and S. Cho, *Materials Today Energy*, 5 (2017) 138-157.
30. L. Li, G. Jiang and J. Ma, *Materials Research Bulletin*, 104 (2018) 53-59.
31. V. Singh, D. Joung, L. Zhai, S. Das, S. Khondaker and S. Seal, *Progress in Materials Science*, 56 (2011) 1178-1271.
32. X. Zhao, H. Li, F. Han, M. Dai, Y. Sun, Z. Song, D. Han and L. Niu, *Journal of Physics and Chemistry of Solids*, 139 (2020) 109301.
33. Y. Wang and C. Huang, *Process Safety and Environmental Protection*, 142 (2020) 295-307.
34. R. Genieser, S. Ferrari, M. Loveridge, S.B. Beattie, R. Beanland, H. Amari, G. West and R. Bhagat, *Journal of Power Sources*, 373 (2018) 172-183.
35. P.W. Abegg, *Molecular Physics*, 30 (1975) 579-596.
36. M.H. Abraham, *Chemical Society Reviews*, 22 (1993) 73-83.
37. D. Jacquemin and C. Adamo, *Chemical Society Reviews*, 42 (2013) 845-856.
38. J. Shin, J. Seo, R. Yaylian, A. Huang and Y. Meng, *International Materials Reviews*, 65 (2019) 356-387.
39. Y.G. Lee, S. Fujiki, C. Jung, N. Suzuki, N. Yashiro, R. Omoda, D.S. Ko, T. Shiratsuchi, T. Sugimoto, S. Ryu, J. Ku, T. Watanabe, Y. Park, Y. Aihara, D. Im and I. Han, *Nature Energy*, 5(2020) 299-308.
40. M. Ue, Role-Assigned Electrolytes: Additives. In: M. Yoshio, R.J. Brodd, A. Kozawa, Lithium-Ion Batteries. *Springer, New York*, (2009) 348-350.
41. Y. Zhao, F. Xie, C. Zhang, R. Kong, S. Feng and J.X. Jiang, *Microporous and Mesoporous Materials*, 240 (2017) 73-79.
42. J.B. Goodenough and H. Lee, *Journal of Solid State Chemistry*, 144 (1999) 220-223.
43. J. Yan, Z. Fan, T. Wei, W. Qian, M. Zhang and F. Wei, *Carbon*, 48 (2010) 3825-3833.
44. M. Toupin, T. Brousse and D. Belanger, *Chemistry of Materials*, 16 (2004) 3184-3190.
45. J. Li, and I. Zhitomirsky, *Materials Chemistry and Physics*, 112 (2008) 525-530.
46. W. Xiao, H. Xia, J.Y.H. Fuh and L. Lu, *Journal of The electrochemical Society*, 156 (2009) A627.
47. M. Wu, L. Zhang, J. Gao, C. Xiao, D. Wang, A. Chen and S. Zhang, *Journal of Electroanalytical Chemistry*, 613 (2008) 125-130.
48. W. Chen, R.B. Rakhi, L. Hu, X. Xie and H.N. Alshareef, *Nano Letters* , 11 (2011) 5165-5172.
49. Y. He, W. Chen, J. Zhou, X. Li, P. Tang, Z. Zhang, J. Fu and E. Xie, *ACS Applied Materials & Interfaces*, 6 (2014) 210-218.
50. P.H. Yang, X. Xiao, Y.Z. Li, Y. Ding, P.F. Qiang, X.H. Tan, W.J. Mai, Z.Y. Lin, W.Z. Wu, T.Q. Li, H.Y. Jin, P.Y. Liu, J. Zhou, C.P. Wong and Z.L. Wang, *ACS Nano*, 7 (2013) 2617-2626.
51. M. Deng, P.J Ho, C.Z. Song, S.A. Chen, J.F. Lee, J.M Chen and K.T. Lu, *Energy & Enviornmental Science*, 7 (2013) 2178-2185.
52. H. Liu, L. Zhang, X. Lang, Y. Yamaguchi, H. Iwasaki, Y. Inoyue, Q. Xue and M. Chen, *Nature nanotechnology*, 1 (2011) 112.
53. P. Li, Y. Yang, E. Shi, Q. Shen, Y. Shang, S. Whu, J. Whi, K. Wang, H. Zhu, Q. Yuan, A. Cao and D. Wu, *ACS Applied Materials & Interfaces* , 6 (2014) 2228-2234.
54. Y. Cheng, S. Lu, H. Zhang, C. Varansi and J. Liu, *Nano Letters*, 12 (2012) 4206-4211.

55. J. Liu, J. Jiang, C. Cheng, H. Li, J. Zhang, G. Hao and H. Fan, *Advanced Materials*, 23 (2011) 2076-2081.
56. Z. Sun, S. Firdoz, E. Yap, L. Li and X. Lu, *Nanoscale*, 5 (2013) 4379-4387.
57. J. Wang, Y. Yang, Z. Huang and F. Kang, *Journal of Materials Chemistry*, 22 (2012) 16943-16949.
58. J. Wang, Y. Yang, Z. Huang and F. Kang, *Electrochimica Acta*, 56 (2011) 9240-9247.
59. P. Lv, P. Zhang, Y. Feng, Y. Li and W. Feng, *Electrochimica Acta*, 78 (2012) 515-523.
60. T. Zhai, F. Wang, M. Yu, S. Xie, C. Liang, C. Li, F. Xiao, R. Tang, Q. Wu, X. Lu and Y. Tong, *Nanoscale*, 5 (2013) 6790-6796.
61. H. Zhang, G. Cao, Z. Wang, Y. Yang, Z. Shi and Z. Gu, *Nano Letters*, 8 (2008) 2664-2668.
62. Y. He, W. Chen, X. Li, Z. Zhang, J. Fu, C. Zhao and E. Xie, *ACS Nano*, 7 (2013) 174-182.
63. J. Yang, E. Khoo, A. Submoja and P. *ACS Nano*, 4 (2010) 4247-4255.
64. A. Burke, *Journal of Power Sources*, 91 (2000) 37-50.
65. P. Simon and Y. Gogotsi, *Nature*, 7 (2008) 845-854.
66. J. Cao, X. Li, Y. Wang, F. Walsh, J.H. Ouyang, D. Jia and Y. Zhou, *Journal of Power Sources*, 293 (2015) 657-674.
67. Y. Huang, J. Liang and Y. Chen, *NanoMicrosmall*, 8 (2012) 1805-1834.
68. K. Wang, S. Zhang, Y. Cheng, X. Yu, B. Tu and H. Tao, *Polyhedron*, 181 (2020) 114436.
69. S. Bharatraj, S.P. Adiga, K.S. Mayya, T. Song, J. Kim and Y. Sung, *Journal of Power Sources*, 474 (2020) 228659.